Title

Positron emission tomography evaluation of oxime countermeasures in live rats using the tracer O-(2-[18F]fluoroethyl)-O-(p-nitrophenyl)methylphosphonate [18F]-VXS

Journal

Annals of the New York Academy of Sciences, 1479(1)

ISSN

0077-8923

Authors

Hayes, Thomas R
Blecha, Joseph E
Chao, Chih-Kai
et al.

Publication Date

2020-11-01

DOI

10.1111/nyas.14363

Peer reviewed

HHS Public Access

Author manuscript

Ann N Y Acad Sci. Author manuscript; available in PMC 2020 November 22.

Published in final edited form as:

Ann N Y Acad Sci. 2020 November ; 1479(1): 180–195. doi:10.1111/nyas.14363.

Positron emission tomography evaluation of oxime countermeasures in live rats using the tracer *O*-(2-[^{18}F]fluoroethyl)-*O*-(*p*-nitrophenyl)methylphosphonate [^{18}F]-VXS

Thomas R. Hayes[1], **Joseph E. Blecha**[1], **Chih-Kai Chao**[2], **Tony L. Huynh**[1], **Henry F. VanBrocklin**[1], **Kurt R. Zinn**[3], **Palmer W. Taylor**[4], **John M. Gerdes**[2], **Charles M. Thompson**[2]

[1]Department of Radiology and Biomedical Imaging, University of California, San Francisco, California.

[2]Department of Biomedical and Pharmaceutical Sciences, University of Montana, Missoula, Montana.

[3]Departments of Radiology, Small Animal Clinical Sciences, and Biomedical Engineering, Institute for Quantitative Health Science and Engineering, Michigan State University, East Lansing, Michigan.

[4]Department of Pharmacology, Skaggs School of Pharmacy and Pharmaceutical Sciences, University of California at San Diego, La Jolla, California

Abstract

Oxime antidotes regenerate organophosphate-inhibited acetylcholinesterase (AChE). Although they share a common mechanism of AChE reactivation, the rate and amount of oxime that enters the brain are critical to the efficacy, a process linked to the oxime structure and charge. Using a platform based on the organophosphate [^{18}F]-VXS as a positron emission tomography tracer for active AChE, the *in vivo* distribution of [^{18}F]-VXS was evaluated after an LD_{50} dose (250 μg/kg) of the organophosphate paraoxon (POX) and following oximes as antidotes. Rats given [^{18}F]-VXS tracer alone had significantly higher radioactivity (two- to threefold) in the heart and lung than rats given LD_{50} POX at 20 or 60 min prior to [^{18}F]-VXS. When rats were given LD_{50} POX followed by 2-PAM (cationic), RS194b (ionizable), or monoisonitrosoacetone (MINA) (neutral), central

Address for correspondence: Charles M. Thompson and John M. Gerdes, Department of Biomedical and Pharmaceutical Sciences, University of Montana, Missoula, MT 59812-1552. chuck.thompson@mso.umt.edu and john.gerdes@umontana.edu.

Author contributions

C.M.T. and J.M.G. designed the tracer and prepared nonradioactive tracer. T.R.H., J.E.B., T.L.H., and H.F.V. developed radiosynthesis and produced [^{18}F]-VX surrogate, performed rodent imaging, biodistribution studies, and blood metabolite analyses. P.T. provided experimental guidance on the administration of oximes. C.-K.C. with J.M.G. performed PET imaging analyses. J.M.G. and C.M.T. wrote the manuscript with contributions from all authors. All authors reviewed the manuscript.

Competing interests

The authors declare no competing interests.

Disclosure

The content is solely the responsibility of the authors and does not necessarily represent the official views of the National Institutes of Health.

Supporting information

Additional supporting information may be found in the online version of this article.

Supplementary Material.

nervous system (CNS) radioactivity returned to levels at or above untreated naive rats (no POX), whereas CNS radioactivity did not increase in rats given the dication oximes HI-6 or MMB-4. MINA showed a significant, pairwise increase in CNS brain radioactivity compared with POX-treated rats. This new *in vivo* dynamic platform using [^{18}F]-VXS tracer measures and quantifies peripheral and CNS relative changes in AChE availability after POX exposure and is suitable for comparing oxime delivery and AChE reactivation in rats.

Keywords

oxime countermeasures; biodistribution; fluorine-18; organophosphate; paraoxon; VX-surrogate tracer; PET imaging

Introduction

Organophosphorus (OP) compounds are small molecules, including insecticides and chemical warfare agents that are toxic because they phosphylate the neurotransmitter-hydrolyzing enzyme acetylcholinesterase (AChE) to form OP–AChE adducts (Fig. 1). OP phosphylation inhibits AChE increasing substrate acetylcholine (ACh) concentration causing overstimulation of receptors leading to cholinergic poisoning. OP exposures require immediate medical attention,[1–5] including a combination of an oxime reactivator, such as pralidoxime (2-PAM) or asoxime chloride (HI-6), a muscarinic receptor antagonist, such as atropine, and an antiseizure medication (midazolam and diazepam) to minimize the morbidity and mortality.[2,5–8] Certain OP–AChE adducts reactivate with oximes (e.g., 2-PAM),[9–16] whereas other OP–AChE adducts undergo aging to form a phosphorus oxyanion (Fig. 1) that is refractory to reactivation.[11,17–22] Mechanistically, oximes are a direct-acting therapeutic restoring AChE to a functional state by removal of the phosphyl group from AChE.[23,24] Although most oximes are attracted to AChE by virtue of a cation charge mimicking ACh, the ionized group limits penetration into the central nervous system (CNS).[24–26] Conversely, high blood levels of cationic oximes can reactivate circulating and peripheral esterases that can protect the CNS from OP injury. Ideally, oxime therapeutics would reactivate both central and peripheral pools of OP-inhibited cholinesterases to effect OP intoxication recovery. A number of cationic oximes, such as 2-PAM, HI-6, trimedoxime bromide (TMB-4), 1,1′-methylenebis[4-[(hydroxyimino)methyl]-pyridinium (MMB4), and obidoxime (Fig. 2), are widely used despite poor penetration into the brain, whereas a neutral oxime like monoisonitrosoacetone (MINA) and ionizable oxime like RS194b (Fig. 2) can penetrate the CNS more easily[27–29] but may not form a strong ionic attraction to AChE.

2-PAM is primarily used in the United States to treat OP exposures, but the ability of a given oxime to reactivate inhibited AChE is typically related to the structure of the OP–AChE adduct,[30,31] and whether or not adduct aging has occurred (Fig. 1). A continued limitation in the assessment of oxime therapeutics is that the restored AChE activity is typically measured in blood,[32] which weakly correlates to the CNS toxicity. A more direct *in vivo* measure of the CNS AChE activity in tissues and the progress of the reactivation would be highly beneficial for the development of more efficacious oxime countermeasures and their respective dosing protocols.

Positron emission tomography (PET) imaging is an established clinical and research technique that quantifies the uptake, distribution, elimination, and metabolism of positron-labeled molecules (tracer and radioligand) in tissues.[33,34] PET imaging is sensitive and can assess pharmacokinetic (PK) and pharmacodynamic (PD) parameters typically using ^{18}F ($t_{1/2}$ = 110 min) or ^{11}C ($t_{1/2}$ = 20 min) isotopically labeled tracers. PET studies that targeted the CNS[35–38] are established and are an excellent choice to assess OP mechanism and oxime therapeutic efficacy because the method can interrogate quantitative tissue distribution *in vivo* in real time. Another advantage of low-mass PET tracers is that uptake is proportional to the target amount but insufficient to produce a pharmacologic effect. Because OPs react only with functional AChE, an OP compound bearing a positron isotope (OP tracer) could report dynamically on the remaining functional AChE levels following an OP exposure and/or the level of reactivated AChE following oxime intervention.

Recently, we reported the preparation, mechanism of action, and *in vivo* biodistribution of the first-in-class OP PET tracer, *O*-(2-[^{18}F]fluoroethyl)-*O*-(*p*-nitrophenyl) methylphosphonate ([^{18}F]-VX surrogate; [^{18}F]-VXS)[39–41] that is a hybrid structure of paraoxon (POX) and the chemical warfare agent VX. [^{18}F]-VXS tracer is a potent covalent inhibitor of AChE[39,42] that in rats distributes rapidly into the CNS and quantitatively reports on available AChE as the [^{18}F]–VXS–AChE adduct.[41] Two key qualities of the [^{18}F]-VXS tracer are (1) it forms a covalent OP–AChE adduct that does not undergo aging to an appreciable extent within the lifetime of the tracer[39] (Fig. 3) and (2) the F–VXS–AChE adduct does not undergo spontaneous reactivation within the lifetime of the tracer but is reactivatable by oximes.[39] An OP PET tracer possessing these features eliminates numerous *in vivo* quantitation complications associated with rapid reactivation as seen with carbamate tracers (reactivation $t_{1/2}$ ~20 minutes).[43]

Overall, the OP–AChE adduct formed from [^{18}F]-VXS is stable such that functional AChE, whether native or restored by oxime, can be potentially correlated to the [^{18}F]–VXS–AChE adduct formed (Figs. 3 and 4). Therefore, [^{18}F]-VXS was selected as a tracer to develop a quantitative PET imaging platform to measure available/functional AChE in live tissues following OP exposure and after intervention with oximes. POX was chosen as the OP challenge agent since it is a potent anticholinesterase inhibitor, affords a predictable toxicological profile, and the diethylphosphoryl–AChE adduct formed by POX (or related diethoxy phosphorylating agents, such as phorate[44]) undergoes reactivation by oximes and does not age in the hours following AChE inhibition.[45]

In this study, the PET biodistribution (bioD) and metabolism of [^{18}F]-VXS was determined under various conditions (Fig. 3). Conditions included (1) dosing of [^{18}F]-VXS alone, with no treatment (referenced as “none”; not shown in Fig. 5), (2) POX exposure at a dose that causes death in 50% of animals (LD_{50}) with treatment of [^{18}F]-VXS at 20 or 60 min after POX (referenced as “20 min” or “60 min”; Fig. 5), or (3) LD_{50} POX exposure followed by an oxime antidote 30 min later (Fig. 5; control is saline or vehicle only), with dosing of [^{18}F]-VXS at 30 min after the oxime and 60 min after POX (oximes: “2-PAM,” “HI-6,” “MINA,” “MMB4,” or “RS194b”). In principle, rats exposed to POX form diethoxyphosphoryl–protein adducts that changes the [^{18}F]-VXS PET biodistribution,

including to the CNS. Similarly, if an oxime antidote reactivated AChE, then the amount of [^{18}F]-VXS in the tissue would correspondingly increase, depending on the oxime.

Experimentally, oximes that successfully displace the diethoxyphosphoryl moiety restore these esterases that can then react with [^{18}F]-VXS tracer to form tracer-labeled AChE adduct allowing quantification relative to no oxime (vehicle or control) treatment. Conversely, oximes that are ineffective at reactivating AChE allow the diethoxyphosphoryl–AChE adduct to remain that does not react with [^{18}F]-VXS and remain unlabeled (Fig. 4). The cationic oximes tested (2-PAM, MMB4, and HI-6) were expected to show reactivation of cholinesterases in blood and peripheral tissues but not the brain, whereas the neutral and ionizable oximes (MINA and RS194b) were presumed to enter the CNS more easily possibly leading to a greater reactivation of CNS AChE. As this study was conducted only in rats, it is worthwhile to note that AChE from other species can be selectively reactivated by different oximes.[46,47]

The mechanisms in Figures 1 and 3, which may include other OP reactive esterases besides AChE, are active *in vivo* within blood, and also peripheral and central tissue domains to various extents (Fig. 6, top row). Thus, specific experiments that comprehensively evaluate these compartments over time are required. Further, a variety of rat group types (Fig. 6, mid-row) are required, including rat cohorts composed as naive, POX exposed (alone, devoid of other treatments), and POX exposed followed by oxime therapeutic. Therefore, an effective platform to simultaneously interrogate the biological compartment and rat group variables demand several different types of parallel quantitative experiments (Fig. 6, last panel) utilizing low tracer [^{18}F]-VXS doses that include (1) arterial blood sampling and radioactivity composition analyses, (2) *ex vivo* tissue bioD radioactivity evaluations, and (3) *in vivo* PET imaging profiling, in which data from each of these experimental sets are compared with the other two. Importantly, since low-mass [^{18}F]-VXS tracer doses are utilized, the blood and tissue measures obtained are derived below AChE target (and related esterases) saturation level(s).

The platform experiments in this study were (1) evaluation of blood and tissue levels of [^{18}F]-VXS tracer in naive rats, baseline determination; (2) appraisal of blood and tissue levels of [^{18}F]-VXS tracer in rats at 20 and 60 min following an LD_{50} dose of POX; and (3) appraisal of blood and tissue levels of [^{18}F]-VXS tracer in animals at 60 min following an LD_{50} dose of POX with oxime intervention performed at 30 min after POX exposure. As outlined in Figure 4, [^{18}F]-VXS reacts only with functional enzyme and not with OP-inhibited or -aged enzymes. Therefore, oximes that displace an OP from an enzyme and restore the activity either in part or full would permit a greater amount of [^{18}F]-VXS to form a tracer–enzyme adduct, resulting in increased radioactivity detection. The rapid penetration of [^{18}F]-VXS into the CNS will enable distinct measures of functional AChE in the brain.[41]

Materials and methods

All solvents, USP-grade solutions, and reagents were purchased as reagent grade or better from Sigma-Aldrich Chemical Company (Milwaukee, WI). Reversed-phase HPLC was performed with a Waters 590 system (Milford, MA) coupled to a Shimadzu SPD UV-Visible

detector (Columbia, MD) and a gamma counting in-line radiation flow detector (Model 105s, CRA; Berkeley, CA). Analytical HPLC data were collected with an SRI PeakSimple, model 304, data system (Torrance, CA), using a semipreparative or analytical reversed-phase HPLC Luna C18(2) columns (Phenomenex®; Torrance, CA). Counting of tissue and blood samples utilized a Hidex automated gamma counter (Turku, Finland). POX (diethyl *p*-nitrophenylphosphate) was prepared in house and purified to >99% before use. The hydrolyzed metabolite *O*-(2-fluoroethyl) methylphosphonic acid was prepared by reaction of *O*-(2-fluoroethyl)-*O*-(*p*-nitrophenyl)methylphosphonate with a 10-fold excess of 1.0 N NaOH in H_2O:CH_3CN (3:1) at room temperature for 3 hours. RS194b HCl salt was a gift of Palmer Taylor (UCSD). [^{18}F]-VXS was synthesized similarly to the procedure described previously.[40] A one-way ANOVA was performed using Microsoft Excel (version 16.16.12) or R (version 3.5.2). A *P*-value < 0.05 was considered statistically significant in data tables and pairwise comparisons.

Dosing, imaging, and processing

Male Sprague–Dawley young adult rats (250–400 g; Charles River, Inc., Skokie, IL) were used for [^{18}F]-VXS biodistribution, blood, and PET imaging studies. Before injection of [^{18}F]-VXS tracer, rats were lightly anesthetized (~1–1.5% isoflurane) and catheters (TERUMO, Surflash I.V. catheter, CE0197) were installed. The i.v. bolus dose of [^{18}F]-VXS (0.71–2.1 mCi, 350–850 μL) was administered via a tail vein catheter followed by a 300-μL saline flush. For imaging, a partial volume correction was not applied, and conservative tissue regions of interest definitions were used. The computed axial tomography (CT) data were acquired in the standard rat model (see Supporting information, online only).

[^{18}F]-VXS tracer analyses following POX challenge and following POX challenge with oxime intervention

Rats were given a dose of 250 μg/kg POX (~LD_{50}) in 10% MeCN/PBS (pH 6.8) via a lateral tail vein catheter followed by a 300-μL saline flush under isoflurane anesthesia. For POX challenge only, at 20 or 60 min, the subjects were given the i.v. bolus dose of [^{18}F]-VXS (0.67–1.6 mCi, 350–900 μL) via a tail vein catheter followed by a 300-μL saline flush and the PET imaging data acquired. For the oxime interventions at 30 min postexposure to POX, the subjects were administered a one-time bolus dose of one of the five following oximes as an intramuscular (i.m.) saline solution: (1) 2-PAMCl^- (30mg/kg); (2) MMB4 2Br^- (77 mg/kg); (3) HI-6 2Cl^- (54 mg/kg); (4) MINA (15 mg/kg); and (5) RS194b (formulated as HCl; 109 mg/kg), or saline as control. At 30 min posttreatment with oxime (60 min postexposure to POX), the subjects were given the i.v. bolus dose of [^{18}F]-VXS (0.78–2.0 mCi, 300–800 μL) via a tail vein catheter followed by a 300-μL saline flush and the PET imaging data acquired over 33 min beginning at the injection of the tracer. Additional experimental details for the tracer synthesis and stability, dosing, arterial sampling, and imaging scan acquisitons and data processing, in addition to statistical analyses[48] with various representations, can be found in Supporting information (online only).

Results and discussion

Arterial blood sampling with the [^{18}F]-VXS tracer

For blood sampling, rats were given a bolus of [^{18}F]-VXS via a tail vein catheter amounting to 0.09–1.7 ng mass of tracer per injection. The tracer dose is far below any level expected to contribute to OP toxicity such that AChE tissue saturation with tracer does not occur. Arterial blood analyses were first conducted in naive rats following [^{18}F]-VXS tracer administration alone to measure parent, metabolite(s), and protein- and RBC-bound fractions from 0.5 to 30 min (Table 1; no POX). Within 1 min, the [^{18}F]-VXS tracer (parent) was rapidly reduced to 0.2% and remained at barely detectable levels for 30 minutes. The radiometabolite ($^{18}FCH_2CH_2O$)(Me)P(O)OH) formed to >10% over the first minute but quickly leveled to approximately 5–6% over the remainder of the sampling period ($P < 0.05$). This metabolite can arise from spontaneous reactivation of phosphylated blood cholinesterases, enzymatic hydrolysis, and/or nonspecific hydrolysis of the tracer. The hydrolytic metabolite [^{18}F]-2-fluorethanol was not identified but may have been converted to fluoride and/or fluoroacetate.[49] The majority of [^{18}F]-VXS tracer concentration produced radioactivity associated with the protein fraction initially at 70% and increasing to 81–82%. The protein fraction is thought to mostly represent phosphylation of butyrylcholinesterase (BuChE), carboxyesterases (carbE), and other blood and serum esterases.[50] Radioactivity was also found associated with red blood cells that remained steady at 13–16% of the total radioactivity and presumably due to tracer phosphylation of RBC AChE and/or entry of the tracer into RBCs. These measures were important to establish baseline levels. The very low amount of mass of injected [^{18}F]-VXS permits OP-reactive esterases that are expressed in high concentrations, such as BChE[51] and CarbE,[50] to react with the low amount of mass of tracer injected.

Arterial blood analyses were conducted at 20 and 60 min with [^{18}F]-VXS in rats after an LD_{50} dose of POX was given. The 20-min time point was selected to identify early-stage changes in the blood distribution of radioactivity following a POX exposure, whereas the 60-min time point was selected to sample a later stage in the POX exposure toxicity and as a function of the oxime treatment (Fig. 5). Results indicate that initial exposure to POX did not alter the amount of parent tracer in blood relative to naive at either 20- or 60-min time points, with only very low levels observed. However, a 2- to 2.5-fold increase in the amount of metabolite relative to naive was found at 0.5–1.0 min in both 20- and 60-min time points that remained elevated relative to naive, yet dropped substantially over the analysis period. Likewise, in POX-treated rats, the RBC radioactivity levels were almost twofold that of untreated subjects, the 20- and 60-min levels were similar, and the RBC-associated radioactivity remained high over the analysis period. The radioactivity level increases in metabolite and RBC fractions in the POX-treated animals relative to untreated rats were offset by a 15–25% overall decrease in the protein fraction; however, the protein fraction increased approximately 10% in each 20- and 60-min treatment group over 30 minutes. The net decrease in the protein fraction relative to naive untreated rats is presumed to be due to POX inhibition of BChE and CarbE that preemptively blocks the tracer from interacting with these esterase proteins. However, the percent radioactivity in RBC was higher after a POX dose versus naive rats and, therefore, the higher levels cannot be due to POX inhibition

of RBC AChE. One possible explanation is that POX inhibition of BChE, CarbE, and nonspecific esterases permits a proportionally greater amount of [^{18}F]-VXS tracer to modify proteins associated with RBC and/or it is possible that a portion of the RBC radioactivity level represents cellular uptake of tracer.

[^{18}F]-VXS tracer was given 60 min after an LD_{50} POX with oxime intervention at 30 min post-POX exposure in order to assess the influence of different oximes on the blood composition (Table 2). Again, the amount of parent tracer in rats treated with oximes following POX exposure (Table 2) was barely detectable (0.1–0.2%), as found for naive and POX-treated. Each of the oxime-treated groups yielded metabolite levels that were higher at the early time points (17–24%) than naive (12%) but on average lower than POX-treated (18–31%). All rat groups showed nearly a twofold drop in metabolite level over the 30-min analysis, but the initial rise in metabolite levels in POX- and POX-oxime–treated groups did not decrease over time and was sustained at a level approximately twice that of naive. Among the oxime-treated rats, MMB4 produced slightly higher metabolite levels and 2-PAM slightly lower metabolite levels although none were significantly different from POX-treated. The difference in metabolite levels in the POX-alone and POX-oxime–treated animals may be due to POX blockade of blood enzymes redirecting a greater amount of [^{18}F]-VXS tracer metabolic breakdown (hydrolysis) rather than covalent modification of esterases.

The protein fractions were similar for all the oxime treatments showing an increase by ~5% over the 30-min experiment duration. By comparison, naive and POX-treated animals showed a 10% increase in the radioactivity associated with the protein fraction over 30 minutes. Naive animals had the largest percent protein fraction associated with radioactivity exceeding 80%—an observation that may be due to the relatively small amount of tracer injected that is attached to serum proteins and esterases. In POX-treated rats, these proteins and enzymes are initially bound or blocked by POX. Radioactivity levels associated with RBCs increased in all the oxime treatment groups after 10 and over 30 min, possibly reflecting the delay in the reactivation of POX-inhibited RBC AChE, although the low levels of parent tracer in blood by 0.5 min suggest that phosphylation of restored RBC AChE seems unlikely. Overall, oxime intervention in POX-treated rats did not dramatically alter the composition of blood radioactivity relative to POX-treated without oxime intervention. The largest change in blood analyte composition occurred between naive subjects and the two POX-treated groups, which is thought to be due to the larger fraction of the ultralow tracer mass dose being bound to serum proteins in the naive subjects.

In vivo *PET imaging tissue evaluations using the [^{18}F]-VXS tracer*

To evaluate the bioD of the [^{18}F]-VXS tracer in live rat tissues, imaging was performed over a 30 min scan period. Radioactivity profiles were summed over 0–30 min and the values reported as the area under the curve (AUC) in the brain, heart, liver, and lungs for naive, POX-treated, and POX-treated with oxime intervention (see Supporting information, online only). Radioactivity levels in different brain regions were also quantified; however, the kidney was not consistently in the scanner field of view due to variations in rat size and relative scanner positioning. In select experiments, PET data were collected in timeframes

over segments 0–5, 0–10, 0–15, and 0–30 min (radioactivity summed) to identify any temporal changes in tracer PK/PD properties. As expected, naive rats given only [^{18}F]-VXS tracer had the highest AUC values in the heart and lung with the lowest levels in the brain (Table 3). The heart values likely reflect a combination in blood, tissue, and RBC-associated radioactivity due to a possible direct attachment of tracer. Lung values were high and similar to the heart but represent the accumulation of tracer-modified BChE[52] and CarbE.[50] The bioD profiling showed proportional increases in units of radioactivity for each 5-min segment analyzed that suggest a radioactivity steady state was achieved early after tracer administration where the initial tissue values are dependent on blood flow. Although brain AUC levels were the lowest, the tracer clearly entered the brain and radioactivity did not wash out over the 30-min scan time. Likewise, the various brain regions showed similar incremental increases in AUC over time (Table 3) with the cerebellum (CE) and midbrain (MB) affording the highest AUC levels. Although regional radioactivity quantification could be hampered by the conservatively defined and small size of rat brain regions adjunct with the limited spatial resolution of the PET scanner, the spatial coregistration of the PET-CT-MR data sets (see Supporting information, online only) is considered a robust established imaging method to afford suitable regional quantification of radioactivity.[33]

To evaluate how a reactive OP compound alters tissue distribution of the tracer bioD, rats were given an LD_{50} dose of POX followed by injection of [^{18}F]-VXS at 20 min or 1 h (Fig. 7; and Supporting information, online only). The 20-min and 1-h time points coincide with the acute intoxication progress of POX, and precede oxime intervention by 10 min and following oxime by 30 minutes. In general, radioactivity analyses differed in tissue levels as compared with naives. The trends in both heart and lung AUC levels decreased by two-thirds at the 20-min time point but recovered to one-third of naive at the 1-h scan time post-POX. The reduction in heart and lung AUC following a POX dose is consistent with the arterial blood and bioD tissue analyses in that POX pretreatment first inhibits blood esterases and CarbE thereby lowering the availability of these enzymes to tracer modification. Correspondingly, liver radioactivity trends were elevated following a POX dose relative to naives, presumably due to a greater unreacted fraction of [^{18}F]-VXS that is available for metabolism (see Supporting information, online only). Inhibition of CNS AChE by an LD_{50} POX dose (cholinergic toxicity) may explain the decrease in brain AUC at both 20-min and 1 h because less functional AChE is available for modification by [^{18}F]-VXS. As a result, the tissue AUC values found using [^{18}F]-VXS after an LD_{50} POX dose may be better to measure reactivation changes because the tracer alone is consumed extensively by enzymes and hence unable to report on the total AChE tracer–adduct distribution.

When the tracer radioactivity was assessed by the brain region (Fig. 8; and Supporting information, online only), the brainstem (BS), CE, and MB showed a large decrease in values within the POX-treated rats relative to naive; whereas, the caudate putamen, frontal cortex, and thalamus were largely unchanged. The decrease in radioactivity in CE and MB regions after POX exposure was expected since LD_{50} POX exposure modifies a larger pool of functional AChE thereby blocking [^{18}F]-VXS tracer–AChE adduct formation. The BS region also showed a large reduction in radioactivity following POX exposure; and these radioactivity levels in naives were not as high as CE and MB. As BS is also rich in AChE,[53] the reduction in radioactivity may be due to initial POX–enzyme interaction along with

regional blood flow changes and/or vascular damage due to POX. To our knowledge, this is the first time that dynamic quantitative measures have been conducted in live rat brain tissues showing that different cerebral regions have been altered to various extents by a nonradioactive LD_{50} OP exposure. For these studies, the brain regions revealed that the CE, MB, and BS might be particularly susceptible to OP exposure and provide an imaging-derived signature of OP exposure. It is also noteworthy that there was little to no difference in the AUCs between the 20-min and 1-h measures, suggesting that POX enters and extensively phosphorylates brain enzymes by 20 minutes.

The [^{18}F]-VXS tracer given to rats after exposure to POX reports on a decrease in radioactivity in tissues relative to naive (tracer only) because POX reacts preemptively with AChE target and another nontarget enzymes. Oximes (Fig. 2) displace the OP phosphyl group from inhibited AChE and other esterases, restoring function and allowing the [^{18}F]-VXS tracer to attach to these proteins and correspondingly increase the radioactivity. Oximes that are unable (or limited) to enter the brain and reactivate POX-inhibited AChE should show radioactivity levels similar to that found in POX-treated rats devoid of oxime, whereas those that enter the brain and restore AChE should show increased CNS levels of radioactivity due to the formation of the [^{18}F]-VXS adducts of the oxime-reactivated AChE and esterases.

Rats were treated with an LD_{50} dose of POX and at 30 min postexposure then administered 2-PAM, HI-6, MINA, MMB4, or RS194b. Oxime reactivation was allowed to proceed for 30 min, at which point tracer [^{18}F]-VXS was injected (1 h post-POX); the rats were then imaged over 30 min and the bioD was evaluated in the brain, heart, liver, lung (Fig. 7; and Supporting information, online only), and various brain regions (Fig. 8; and Supporting information, online only). It should be noted that despite being given an LD_{50} dose of POX, many symptoms typically associated with OP toxicity were not observed owing to the protective effect of isoflurane.[54]

The box plots (Figs. 7 and 8; Supporting information, online only) highlight the statistical significance variations, data spread, and provide a means to identify any data outliers, and are particularly useful for comparing distributions across groups, which is important in the determination of oxime efficacy. In peripheral tissues, the radioactivity AUC values following the addition of each oxime were higher in the heart and lung than found in the 1-h POX-only group (Fig. 7), indicating a favorable reactivation effect of oxime on these tissues (Fig. 7; and Supporting information, online only). Administration of each of the oximes led to a similar level of radioactivity in the heart representing an increase relative to POX-treated subjects; however, these values were substantially lower than naive. The increase in heart radioactivity following oxime is presumably due to reactivation of RBC and heart tissue AChE where the trend is similar to the increases observed in the profiles found in the *ex vivo* metabolite study (Table 2). However, heart radioactivity levels remained 30–35% lower than those in naive rats (see Supporting information, online only), which might represent incomplete reactivation of tissue and blood esterases over the brief 30-min oxime therapeutic window examined in this study. Moreover, there was no statistical difference in heart tissue AUC between the charged (2-PAM, HI-6, and MMB4) and uncharged MINA and ionizable RS194b oximes (Fig. 7).

Liver levels were differentially affected depending on the oxime. The 20-min and 1-h POX-treated rats showed a 100% and 50% increase, respectively, in liver radioactivity as compared with naive, albeit tissue radioactivity errors were large. The dication oximes HI-6 and MMB4 afforded liver levels similar to naive, whereas the neutral oximes MINA and RS194b gave slightly elevated levels of radioactivity. Treatment with 2-PAM gave radioactive liver levels almost double that of naive and were similar to POX-treated at 20 min, but again with errors (see Supporting information, online only). On the basis of the blood analyses, the liver radioactivity most likely represents a combination of metabolites and protein-bound fractions. The elevated radioactivity level found in the liver after 2-PAM was given may represent oxime effectiveness in restoring circulating esterases inhibited by [^{18}F]-VXS, thereby forming tracer metabolite(s). Lung levels closely paralleled heart with similar increases relative to POX-treated but significantly lower than naive. In the lung, the action of an oxime to restore CarbE and related esterases may be a contributor to the increasing radioactivity levels, although there was a large difference between the 20-min and 1-h POX-treated time points, possibly representing the spontaneous reactivation of POX-inhibited CarbE and butyrylcholinesterase before the oxime dose. Still, radioactivity levels in the lung were higher with oxime administration relative to POX-only rats at 1 h, and none of the oximes evaluated restored the radioactivity level to that of naive.

Radioactivity AUC values varied in regional brain tissues (see Supporting information, online only) depending on the oxime administered (Fig. 8). Naive rats showed an AUC = ~40, whereas POX-treated rats decreased to AUC = ~32.1 ± 3.1 by 20 min and to AUC = 34.4 ± 1.7 at 1 hour. The 1-h post-POX value (AUC = ~34.4) was used as a baseline value to assess the effectiveness of the various oximes. The results show a clear difference in AUCs obtained for the doubly charged, singly charged, and uncharged/ionizable oxime antidotes as follows. The doubly charged oximes HI-6 (33.6 ± 0.8) and MMB4 (29.5 ± 1.0) yielded the lowest levels of radioactivity in the brain indicating that little or no CNS AChE was reactivated over the 30-min duration of oxime action. This result was somewhat expected as these doubly charged molecules are thought to poorly penetrate the CNS.

Rats given the singly charged oxime 2-PAM following POX, however, showed a clear change in brain radioactivity with the AUC = 39.3 ± 2.2 (16% increase) that is thought to correlate with some measurable AChE reactivation. Although the charge of 2-PAM has been argued as a limitation to brain entry, some studies found that 2-PAMmay enter the brain and be of high therapeutic value especially following an OP exposure.[55,56] Our results suggest that 2-PAM increases functional enzymes in the CNS as indicated by the total radioactivity measured following an [^{18}F]-VXS tracer dose. The well-established therapeutic use of 2-PAM in the SOC protocol also speaks of its favorable therapeutic action, in which the results of the present PET imaging study suggest that the 2-PAM mechanism of action is detectable in the brain in addition to peripheral tissues.

The ionizable oxime RS194b[57–60] (AUC = 40.1 ± 3.2; charged at physiological pH) and neutral oxime MINA (AUC = 47.1 ± 3.3) led to large radioactivity level changes in the CNS relative to the 1-h POX time point (Fig. 7; and Supporting information, online only). Rats given RS194b, an oxime designed to exist in both neutral and charged forms, led to an increased radioactivity level for LD_{50} POX alone and returned brain radioactivity levels

equal to naive subjects indicating CNS penetration by this novel oxime therapeutic. RS194b lacks a structurally localized cation moiety that typically attracts and anchors the oxime to cholinesterases, but the imaging results were superior to the doubly charged oximes and comparable to 2-PAM; however, RS194b was given at a higher dose than the other oximes. The most surprising results were found for rats given the uncharged oxime MINA after an LD_{50} POX dose. The brain radioactivity levels in MINA-treated rats resulted in an ~40% increase in AUC versus POX-only–treated animals, and 50% greater than that found for the dication oximes (Fig. 7; and Supporting information, online only). As a small uncharged molecule, MINA is able to enter the brain; however, the lack of a cation moiety also diminishes attraction to cation-seeking cholinesterases. The high radioactivity AUC observed after the [^{18}F]-VXS tracer dose may therefore be a result of a combination of MINA-reactivated cholinesterases and possibly other serine hydrolases. Unlike the other oximes, the MINA brain radioactivity level greatly exceeds that found for both POX-treated and naive rats, further emphasizing that the low-mass tracer dose is not allowing the saturation of brain AChE concentration. For all the oximes examined, it is important to note that extending the reactivation time beyond 30 min before tracer dose may show greater improvements than those reported here.

As noted, naive CNS radioactivity levels reflect the ultralow-mass dose of [^{18}F]-VXS, whereas POX-treated CNS radioactivity represents a level of targets blocked by a larger concentration of LD_{50} POX. MINA administration after POX exceeds these values because it effectively reactivates POX-inhibited AChE in the brain, thereby allowing [^{18}F]-VXS to attach to reactivated enzyme; whereas peripheral enzymes, such as CarbE, remain blocked in part or full by POX allowing more [^{18}F]-VXS to elude these enzymes resulting in more radioactivity entering the brain. This supposition is further supported, in part, by the finding that MINA-treated POX rats show lower radioactivity levels in the lung, heart, and blood than naive.

The differences between the *in vivo* radioactivity brain distributions in naive, POX-treated, and oxime intervention is shown by quantitative PET imaging views (Fig. 9). The typical PET views are 30 min summed radioactivity coregistered with CT data for anatomical landmarks after baseline [^{18}F]-VXS tracer injection, at a 1-h post-POX dose, and after MINA (Fig. 9). The PET sagittal views reflect the distribution data in Supporting information (tabular data in support of Fig. 8, online only) that indicate the amount of radioactivity in naive subjects decreases after POX administration due to blocked enzymes, but then the radioactivity levels increase substantively when MINA is given to reactivate these enzymes.

In general, regional brain analyses followed the same trend as the whole brain (Fig. 8; and Supporting information in support of Fig. 8, online only). The dication oximes, HI-6 and MMB4, led to radioactivity values that were distributed across brain regions at levels similar to untreated (naive, 1 h post-POX), showing nearly no effect. Conversely, intervention with 2-PAM or RS194b led to a clear elevation in brain radioactivity across all five cerebral regions with the largest change occurring in MB. The addition of MINA led to highly significant increases across all brain regions, most notably the AChE-rich BS[53] and MB regions that revealed a 50% increase in radioactivity versus POX-treated devoid of oxime at

1 h (Supporting information, online only). Based on the increase in CNS radioactivity following [^{18}F]-VXS injection, the *in vivo* quantitative dynamic PET studies reveal that MINA is the most effective reactivator of POX-modified proteins in the CNS at least in the early stages (30 min) after exposure. Oximes 2-PAM and RS194b also performed well as reactivators of POX-modified enzymes under this experimental paradigm.

An important aspect of the study was the finding that a majority of the radioactivity resulting from [^{18}F]-VXS tracer given to naive rats (baseline) was found in lung tissue. This observation was attributed to the reaction of the tracer with CarbE and/or BChE. This suggested that the more appropriate comparative baseline value for CNS tissues was the LD_{50} POX at 1 h that reacts with the available CarbE/BChE, thereby allowing enhanced concentrations of free [^{18}F]-VXS tracer to penetrate and measure AChE interactions in both CNS tissues and peripheral tissues.

In summary, to quantitatively appraise OP reactive mechanisms operating concurrently *in vivo* within blood, and also peripheral and central tissues to various extents, a paradigm composed of specific blood, bioD, and PET imaging experiments that comprehensively evaluate these compartments over time with the novel PET tracer [^{18}F]-VXS has been utilized. Using low-mass tracer [^{18}F]-VXS doses that do not saturate target, this highly useful *in vivo* dynamic tracer was found to quantitatively differentiate POX bioD and effectively interrogate oxime efficacy in a rat model. We consider the *in vivo* dynamic platform suitable for measuring and comparing oxime effectiveness in live rats. This new tracer platform not only measures and quantifies peripheral and CNS changes as a result of OP exposure but can also report on the amount of functional enzyme available in tissues before and after oxime therapeutic antidotes are given. Hence, efforts to expand the platformin other animal species, including primates, are ongoing and those results will be reported in due course. With the examination of new and existing oximes, pretreatments, and scavengers to counteract the OP exposures and toxicity,[1,2,7,8,61–67] this platform deploying quantitative OP tracer PET imaging will help to ascertain the utility of these new candidate therapeutics.

Supplementary Material

Refer to Web version on PubMed Central for supplementary material.

Acknowledgments

Research reported in this publication was supported by the National Institute of Neurological Disorders and Stroke of the National Institutes of Health under Award Number U01NS092495.We are also grateful for support from the NIH and the expert radiochemical technical assistance of Ms. Salma Jivan of the Department of Radiology and Biomedical Imaging at the University of California, San Francisco.

References

1. Bajgar J 2004 Organophosphates/nerve agent poisoning: mechanism of action, diagnosis, prophylaxis, and treatment. Adv. Clin. Chem 38: 151–216. [PubMed: 15521192]
2. Bajgar J, Kuca K, Jun D, et al. 2007 Cholinesterase reactivators: the fate and effects in the organism poisoned with organophosphates/nerve agents. Curr. Drug Metab 8: 803–809. [PubMed: 18220560]

3. Krivoy A, Layish I, Rotman E, et al. 2005 OP or not OP: the medical challenge at the chemical terrorism scene. Prehospital Disaster Med. 20: 155–158. [PubMed: 16018502]
4. Sidell FR 1994 Clinical effects of organophosphorus cholinesterase inhibitors. J. Appl. Toxicol 14: 111–113. [PubMed: 8027505]
5. Sidell FR & Borak J 1992 Chemical warfare agents: II. Nerve agents. Ann. Emerg. Med 21: 865–871. [PubMed: 1610046]
6. Barthold CL & Schier JG 2005 Organic phosphorus compounds—nerve agents. Crit. Care Clin 21: 673–689, v–vi. [PubMed: 16168308]
7. Kovacic P 2003 Mechanism of organophosphates (nerve gases and pesticides) and antidotes: electron transfer and oxidative stress. Curr. Med. Chem 10: 2705–2709. [PubMed: 14529460]
8. Petrikovics I, Papahadjopoulos D, Hong K, et al. 2004 Comparing therapeutic and prophylactic protection against the lethal effect of paraoxon. Toxicol. Sci 77: 258–262. [PubMed: 12857941]
9. Ashani Y, Leader H, Rothschild N, et al. 1998 Combined effect of organophosphorus hydrolase and oxime on the reactivation rate of diethylphosphoryl-acetylcholinesterase conjugates. Biochem. Pharmacol 55: 159–168. [PubMed: 9448738]
10. Langenberg JP, De Jong LP, Otto MF, et al. 1988 Spontaneous and oxime-induced reactivation of acetylcholinesterase inhibited by phosphoramidates. Arch. Toxicol 62: 305–310. [PubMed: 3240095]
11. Lanks KW & Seleznick MJ 1981 Spontaneously reactivation of acetylcholinesterase inhibited by diisopropylfluorophosphate. Biochim. Biophys. Acta 660: 91–95. [PubMed: 7272315]
12. Lieske CN, Clark JH, Meyer HG & Lowe JR 1980 Spontaneous and induced reactivation of eel acetylcholinesterase inhibited by three organophosphinates. Pestic. Biochem. Physiol 13: 205–212.
13. Wilson BW, Hooper MJ, Hansen ME, et al. 1992 Reactivation of organophosphorus inhibited AChE with oximes In Organophosphates: Chemistry, Fate, and Effects. Chambers JE & Levi PE, Eds.: 107–137. Academic Press, Inc, San Diego, CA.
14. Berkman CE, Ryu S, Quinn DA, et al. 1993 Kinetics of the postinhibitory reactions of acetylcholinesterase poisoned by chiral isomalathion: a surprising nonreactivation induced by the RP stereoisomers. Chem. Res. Toxicol 6: 28–32. [PubMed: 8448346]
15. Berman A, Ahn DJ, Lio A, et al. 1995 Total alignment of calcite at acidic polydiacetylene films: cooperativity at the organic–inorganic interface. Science 269: 515–518. [PubMed: 17842362]
16. Ryu SM, Lin J&Thompson CM 1991Comparative anticholinesterase potency of chiral isoparathion methyl. Chem. Res. Toxicol 4: 517–520. [PubMed: 1793798]
17. Barak R, Ordentlich A, Barak D, et al. 1997 Direct determination of the chemical composition of acetylcholinesterase phosphonylation products utilizing electrospray-ionization mass spectrometry. FEBS Lett. 407: 347–352. [PubMed: 9175882]
18. Elhanany E, Ordentlich A, Dgany O, et al. 2001 Resolving pathways of interaction of covalent inhibitors with the active site of acetylcholinesterases: MALDI-TOF/MS analysis of various nerve agent phosphyl adducts. Chem. Res. Toxicol 14: 912–918. [PubMed: 11453739]
19. George KM, Schule T, Sandoval LE, et al. 2003 Differentiation between acetylcholinesterase and the organophosphate-inhibited form using antibodies and the correlation of antibody recognition with reactivation mechanism and rate. J. Biol. Chem 278: 45512–45518. [PubMed: 12933813]
20. Millard CB, Kryger G, Ordentlich A, et al. 1999 Crystal structures of aged phosphonylated acetylcholinesterase: nerve agent reaction products at the atomic level. Biochemistry 38: 7032–7039. [PubMed: 10353814]
21. Ordentlich A, Barak D, Kronman C, et al. 1999 Exploring the active center of human acetylcholinesterase with stereomers of an organophosphorus inhibitor with two chiral centers. Biochemistry 38: 3055–3066. [PubMed: 10074358]
22. Wallace KB & Herzberg U 1988 Reactivation and aging of phosphorylated brain acetylcholinesterase from fish and rodents. Toxicol. Appl. Pharmacol 92: 307–314. [PubMed: 3341039]
23. Shih TM, Skovira JW, O'Donnell JC, et al. 2009 Evaluation of nine oximes on *in vivo* reactivation of blood, brain, and tissue cholinesterase activity inhibited by organophosphorus nerve agents at lethal dose. Toxicol. Mech. Methods 19: 386–400. [PubMed: 19778239]

24. Shih TM, Skovira JW, O'Donnell JC, et al. 2010 *In vivo* reactivation by oximes of inhibited blood, brain and peripheral tissue cholinesterase activity following exposure to nerve agents in guinea pigs. Chem. Biol. Interact 187: 207–214. [PubMed: 20223229]
25. Ahn K, Smith SE, Liimatta MB, et al. 2011 Mechanistic and pharmacological characterization of PF-04457845: a highly potent and selective fatty acid amide hydrolase inhibitor that reduces inflammatory and noninflammatory pain. J. Pharmacol. Exp. Ther 338: 114–124. [PubMed: 21505060]
26. Shih TM, Skovira JW, O'Donnell JC, et al. 2010 Treatment with tertiary oximes prevents seizures and improves survival following sarin intoxication. J. Mol. Neurosci 40: 63–69. [PubMed: 19680820]
27. Bedford CD, Howd RA, Dailey OD, et al. 1986 Nonquaternary cholinesterase reactivators. 3. 3(5)-Substituted 1,2,4-oxadiazol-5(3)-aldoximes and 1,2,4-oxadiazole-5(3)-thiocarbohydroximates as reactivators of organophosphonate-inhibited eel and human acetylcholinesterase *in vitro*. J. Med. Chem 29: 2174–2183. [PubMed: 3783578]
28. Bedford CD, Miura M, Bottaro JC, et al. 1986 Nonquaternary cholinesterase reactivators. 4. Dialkylaminoalkyl thioesters of alpha-keto thiohydroximic acids as reactivators of ethyl methylphosphonyl- and 1,2,2-trimethylpropyl methylphosphonyl-acetylcholinesterase *in vitro*. J. Med. Chem 29: 1689–1696. [PubMed: 3746817]
29. Okuno S, Sakurada K, Ohta H, et al. 2008 Blood–brain barrier penetration of novel pyridinealdoxime methiodide (PAM)-type oximes examined by brain microdialysis with LC-MS/MS. Toxicol. Appl. Pharmacol 227: 8–15. [PubMed: 17964625]
30. Wilhelm CM, Snider TH, Babin MC, et al. 2014 A comprehensive evaluation of the efficacy of leading oxime therapies in guinea pigs exposed to organophosphorus chemical warfare agents or pesticides. Toxicol. Appl. Pharmacol 281: 254–265. [PubMed: 25448441]
31. Wilhelm CM, Snider TH, Babin MC, et al. 2018 Evaluating the broad-spectrum efficacy of the acetylcholinesterase oximes reactivators MMB4 DMS, HLö-7 DMS, and 2-PAM Cl against phorate oxon, sarin, and VX in the Hartley guinea pig. Neurotoxicology 68: 142–148. [PubMed: 30056178]
32. Padilla S 1995 Regulatory and research issues related to cholinesterase inhibition. Toxicology 102: 215–220. [PubMed: 7482556]
33. Ametamey SM, Honer M & Schubiger PA 2008 Molecular imaging with PET. Chem. Rev 108: 1501–1516. [PubMed: 18426240]
34. Timchalk C, Nolan RJ, Mendrala AL, et al. 2002 A physiologically based pharmacokinetic and pharmacodynamic (PBPK/PD) model for the organophosphate insecticide chlorpyrifos in rats and humans. Toxicol. Sci 66: 34–53. [PubMed: 11861971]
35. Borsook D, Becerra L & Fava M 2013 Use of functional imaging across clinical phases in CNS drug development. Transl. Psychiatry 3: e282. [PubMed: 23860483]
36. Gerdes JM, James S, Ahmed SA, et al. 2013 A novel high affinity F-18 organophosphonate tracer for CNS acetylcholinesterase. J. Nucl. Med 54: 323.
37. Soares HD 2010 The use of mechanistic biomarkers for evaluating investigational CNS compounds in early drug development. Curr. Opin. Investig. Drugs 11: 795–801.
38. Wong DF, Tauscher J & Grunder G 2009 The role of imaging in proof of concept for CNS drug discovery and development. Neuropsychopharmacology 34: 187–203. [PubMed: 18843264]
39. Chao CK, Ahmed SK, Gerdes JM, et al. 2016 Novel organophosphate ligand O-(2-fluoroethyl)-o-(p-nitrophenyl)methylphosphonate: synthesis, hydrolytic stability and analysis of the inhibition and reactivation of cholinesterases. Chem. Res. Toxicol 29: 1810–1817. [PubMed: 27551891]
40. Neumann KD, Thompson CM, Blecha JE, et al. 2017 An improved radiosynthesis of O-(2-[18 F]fluoroethyl)-O-(p-nitrophenyl)methylphosphonate: a first-in-class cholinesterase PET tracer. J. Labelled Comp. Radiopharm 60: 337–342. [PubMed: 28406525]
41. James SL, Ahmed SK, Murphy S, et al. 2014 A novel fluorine-18 beta-fluoroethoxy organophosphate positron emission tomography imaging tracer targeted to central nervous system acetylcholinesterase. ACS Chem. Neurosci 5: 519–524. [PubMed: 24716794]

42. Kaleem Ahmed S, Belabassi Y, Sankaranarayanan L, et al. 2013 Synthesis and anti-acetylcholinesterase properties of novel beta- and gamma-substituted alkoxy organophosphonates. Bioorg. Med. Chem. Lett 23: 2048–2051. [PubMed: 23453838]
43. Planas AM, Crouzel C, Hinnen F, et al. 1994 Rat brain acetylcholinesterase visualized with [11C]physostigmine. Neuroimage 1: 173–180. [PubMed: 9343568]
44. Moyer RA, McGarry KG Jr., Babin MC, et al. 2018 Kinetic analysis of oxime-assisted reactivation of human, guinea pig, and rat acetylcholinesterase inhibited by the organophosphorus pesticide metabolite phorate oxon (PHO). Pestic. Biochem. Physiol 145: 93–99. [PubMed: 29482737]
45. Eyer P 2003 The role of oximes in the management of organophosphorus pesticide poisoning. Toxicol. Rev 22: 165–190. [PubMed: 15181665]
46. Worek F, Aurbek N, Wille T, et al. 2011 Kinetic prerequisites of oximes as effective reactivators of organophosphate-inhibited acetylcholinesterase: a theoretical approach. J. Enzyme Inhib. Med. Chem 26: 303–308. [PubMed: 20807085]
47. Worek F, Reiter G, Eyer P, et al. 2002 Reactivation kinetics of acetylcholinesterase from different species inhibited by highly toxic organophosphates. Arch. Toxicol 76: 523–529. [PubMed: 12242610]
48. R Development Core Team. 2010 R: a language and environment for statistical computing. Vienna, Austria: R Foundation for Statistical Computing http://www.R-project.org. (September 2019).
49. Tecle B & Casida JE 1989 Enzymatic defluorination and metabolism of fluoroacetate, fluoroacetamide, fluoroethanol, and (−)-erythro-fluorocitrate in rats and mice examined by 19F and 13C NMR. Chem. Res. Toxicol 2: 429–435. [PubMed: 2519733]
50. Dettbarn WD, Yang ZP & Milatovic D 1999 Different role of carboxylesterases in toxicity and tolerance to paraoxon and DFP. Chem. Biol. Interact 119–120: 445–454.
51. Lockridge O, Duysen EG & Masson P 2013 Butyrylcholinesterase: overview, structure, and function In Anticholinesterase Pesticides: Metabolism, Neurotoxicity, and Epidemiology. Satoh T & Gupta RC, Eds.: 25–41. John Wiley & Sons, Hoboken, NJ.
52. Jbilo O, Bartels CF, Chatonnet A, et al. 1994 Tissue distribution of human acetylcholinesterase and butyrylcholinesterase messenger RNA. Toxicon 32: 1445–1457. [PubMed: 7886701]
53. Strauss V, Rey Moreno MC, Vogt J, et al. 2017 Acetylcholinesterase measurement in various brain regions and muscles of juvenile, adolescent, and adult rats. Toxicol. Mech. Methods 27: 666–676. [PubMed: 28671028]
54. Krishnan JKS, Figueiredo TH, Moffett JR, et al. 2017 Brief isoflurane administration as a postexposure treatment for organophosphate poisoning. Neurotoxicology 63: 84–89. [PubMed: 28939237]
55. Firemark H, Barlow CF & Roth LJ 1964 The penetration of 2-PAM-C14 into brain and the effect of cholinesterase inhibitors on its transport. J. Pharmacol. Exp. Ther 145: 252–265. [PubMed: 14214425]
56. Sakurada K, Matsubara K, Shimizu K, et al. 2003 Pralidoxime iodide (2-PAM) penetrates across the blood–brain barrier. Neurochem. Res 28: 1401–1407. [PubMed: 12938863]
57. Rosenberg YJ, Mao L, Jiang X, et al. 2017 Postexposure treatment with the oxime RS194B rapidly reverses early and advanced symptoms in macaques exposed to sarin vapor. Chem. Biol. Interact 274: 50–57. [PubMed: 28693885]
58. Kovarik Z, Macek N, Sit RK, et al. 2013 Centrally acting oximes in reactivation of tabun-phosphoramidated AChE. Chem. Biol. Interact 203: 77–80. [PubMed: 22960624]
59. Radic Z, Sit RK, Kovarik Z, et al. 2012 Refinement of structural leads for centrally acting oxime reactivators of phosphylated cholinesterases. J. Biol. Chem 287: 11798–11809. [PubMed: 22343626]
60. Sit RK, Radic Z, Gerardi V, et al. 2011 New structural scaffolds for centrally acting oxime reactivators of phosphylated cholinesterases. J. Biol. Chem 286: 19422–19430. [PubMed: 21464125]
61. Cadieux CL, Wang H, Zhang Y, et al. 2016 Probing the activity of a non-oxime reactivator for acetylcholinesterase inhibited by organophosphorus nerve agents. Chem. Biol. Interact 259: 133–141. [PubMed: 27062893]

62. Cerasoli DM, Griffiths EM, Doctor BP, et al. 2005 In vitro and in vivo characterization of recombinant human butyrylcholinesterase (Protexia) as a potential nerve agent bioscavenger. Chem. Biol. Interact 157–158: 363–365.

63. Lushchekina S & Masson P 2018 Catalytic bioscavengers against organophosphorus agents: mechanistic issues of self-reactivating cholinesterases. Toxicology 409: 91–102. [PubMed: 30056174]

64. Lushchekina SV, Schopfer LM, Grigorenko BL, et al. 2018 Optimization of cholinesterase-based catalytic bioscavengers against organophosphorus agents. Front. Pharmacol 9: 211. [PubMed: 29593539]

65. Masson P & Lushchekina SV 2016 Emergence of catalytic bioscavengers against organophosphorus agents. Chem. Biol. Interact 259: 319–326. [PubMed: 26899146]

66. Franjesevic AJ, Sillart SB, Beck JM, et al. 2019 Resurrection and reactivation of acetylcholinesterase and butyrylcholinesterase. Chemistry 25: 5337–5371. [PubMed: 30444932]

67. Zhuang Q, Young A, Callam CS, et al. 2016 Efforts toward treatments against aging of organophosphorus-inhibited acetylcholinesterase. Ann. N.Y. Acad. Sci 1374: 94–104. [PubMed: 27327269]

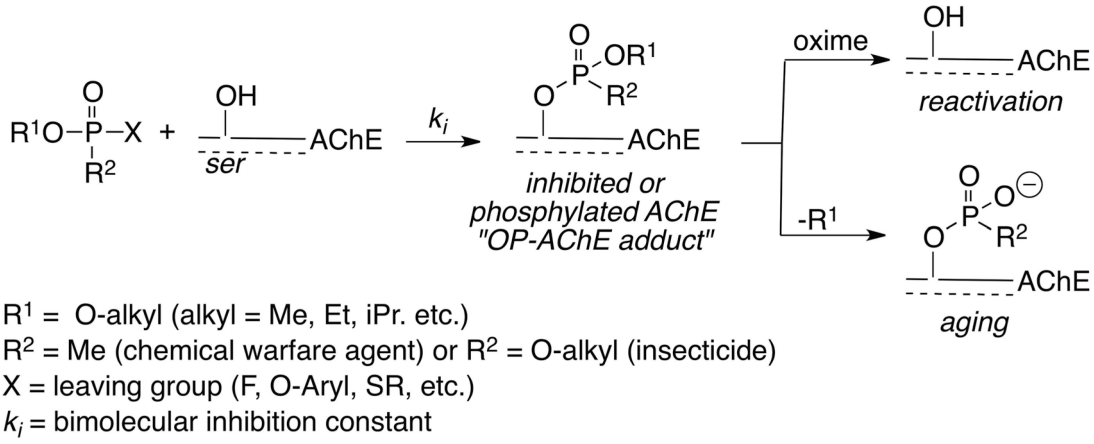

Figure 1.
OP inhibition of AChE and aging of AChE.

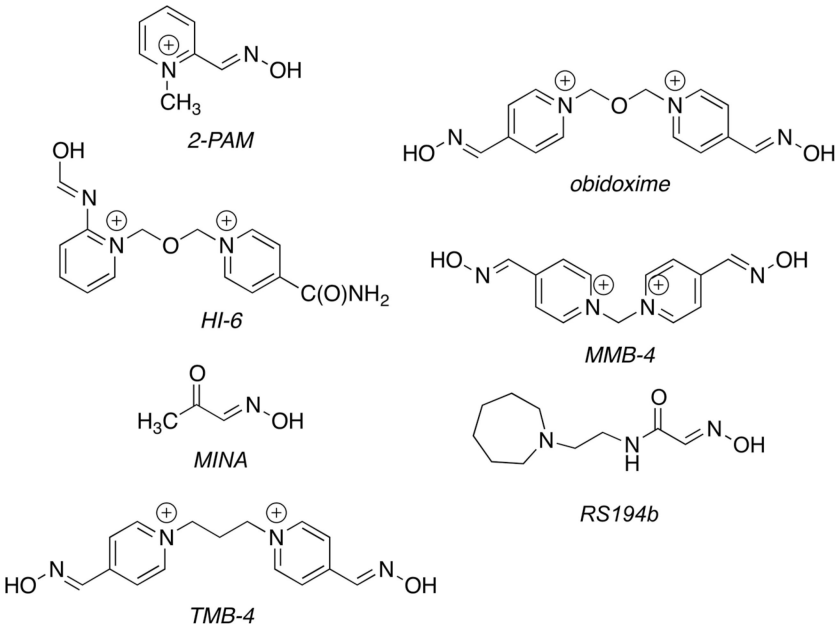

Figure 2.
Structures of representative oximes.

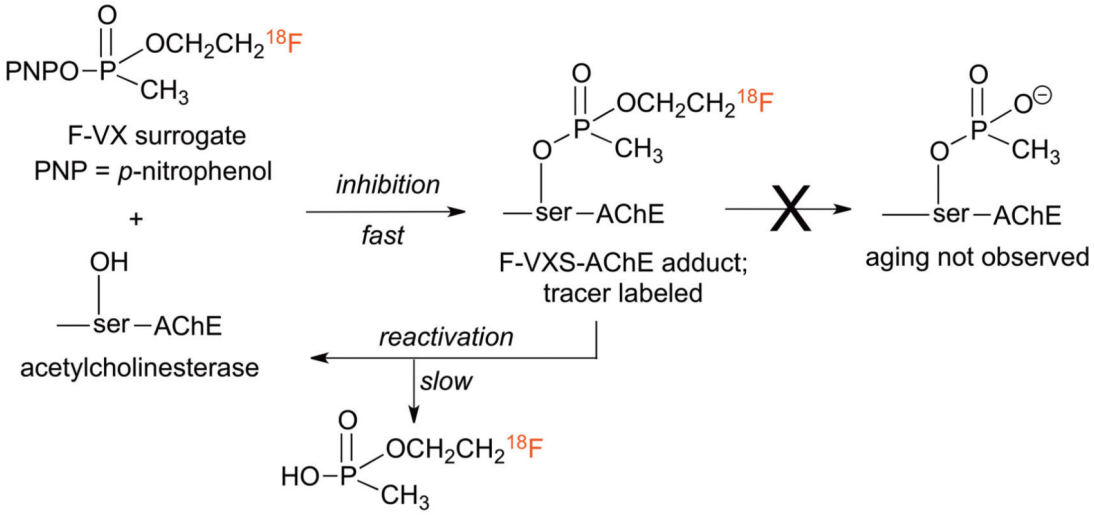

Figure 3.
Mechanisms of AChE interaction with [^{18}F]-VXS.

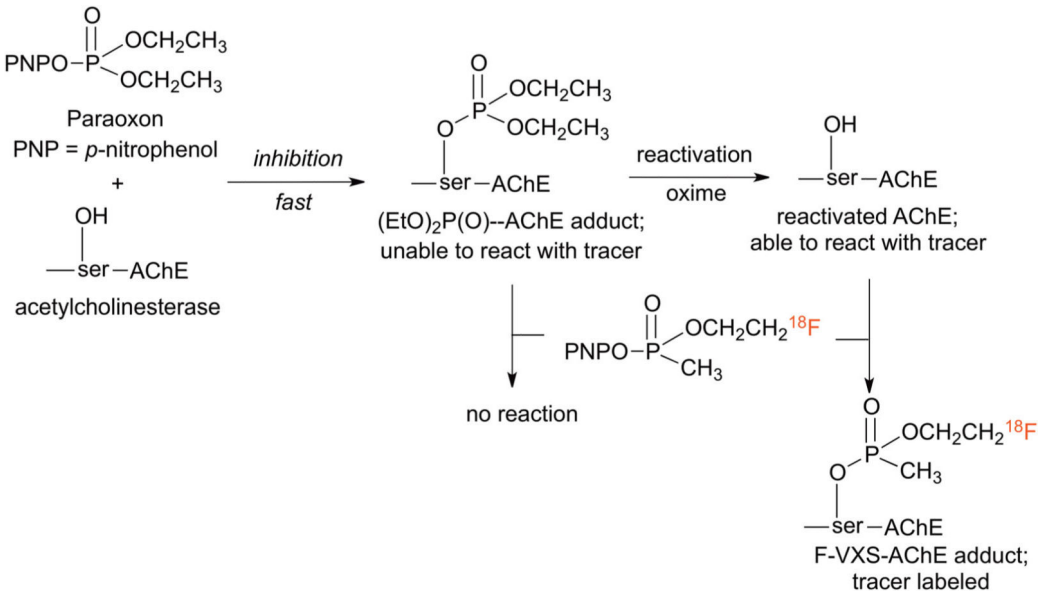

Figure 4.

The use of [^{18}F]-VXS tracer to determine the amount of reactivation following POX inhibition.

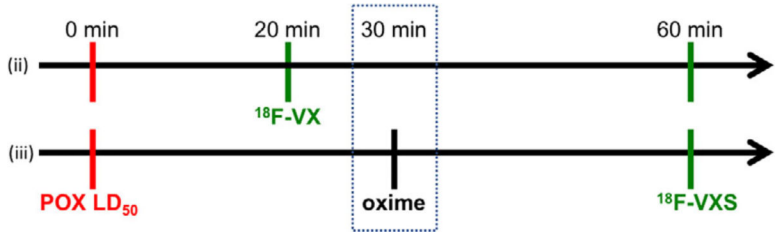

Figure 5.

Experimental timelines used to assess POX exposure; (ii) tracer given after POX exposure only; (iii) tracer given after POX exposure and subsequent oxime therapy.

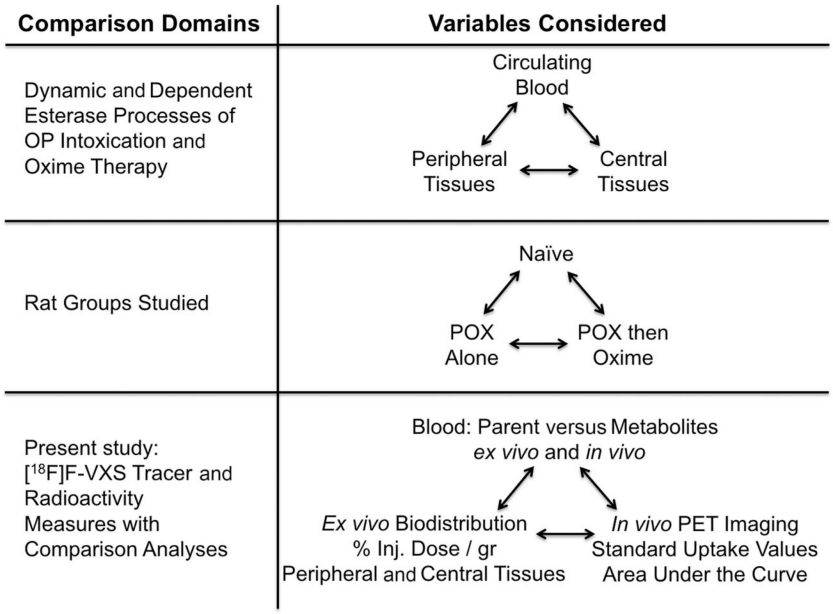

Figure 6.

Dynamic-dependent biological processes (upper row) and experimental paradigms (two lower rows) to interrogate OP intoxication and oxime therapies in rats using tracer [^{18}F]-VXS.

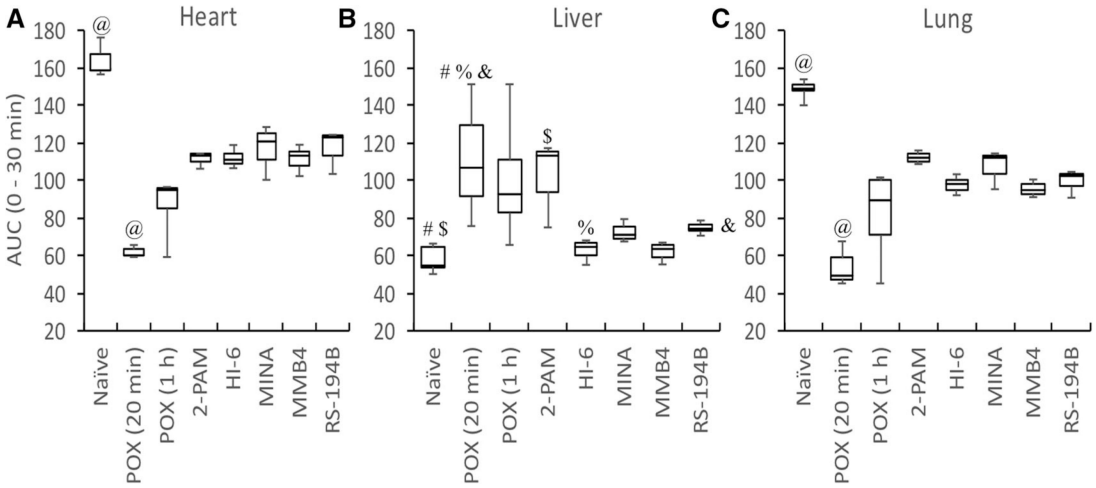

Figure 7.

Box plots showing the area under the curve (AUC) radioactivity distributions from 0 to 30 min in heart (A), liver (B), and lung (C) peripheral tissues for the naive, POX-treated, and oxime treatment groups after [^{18}F]-VXS tracer injection. Boxes depict median (bold line), maximum (upper tick), minimum (lower tick), and first and third quartiles (box height). @ indicates a significantly different value from other treatment groups. # $ % & indicate a significant pairwise difference (see Supporting information for additional statistical representations, online only).

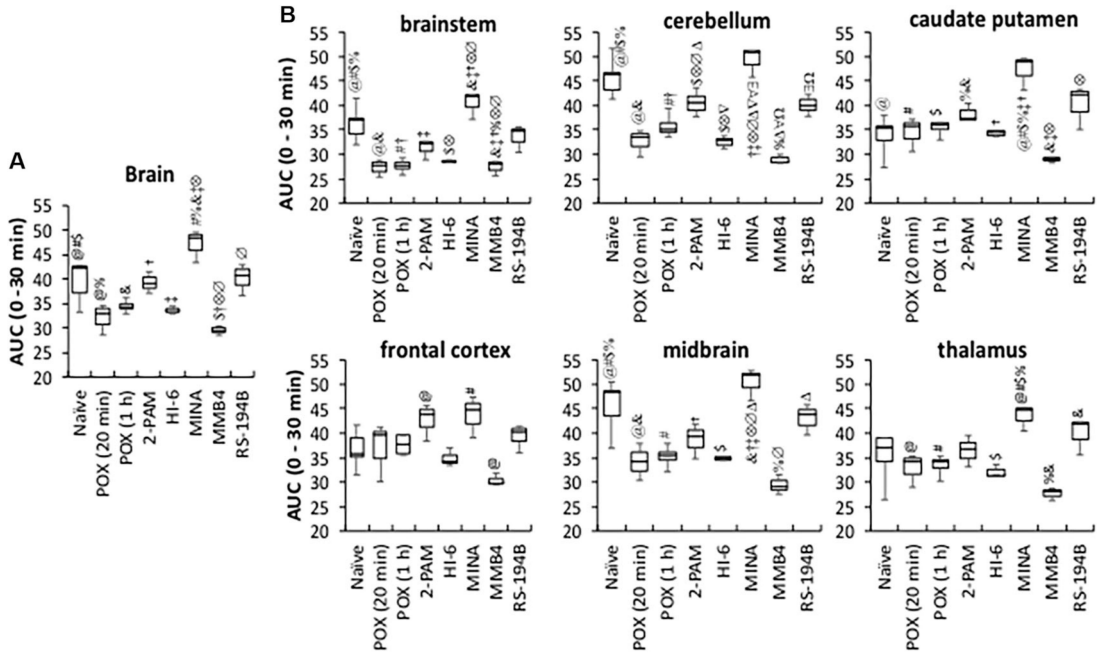

Figure 8.

Box plots showing the area under the curve (AUC) radioactivity distributions from0 to 30-min in whole brain (A) and brain regions (B) for the naive, POX-treated, and oxime treatment groups after [^{18}F]-VXS injection. Boxes depict median (bold line), maximum (upper tick), minimum (lower tick), and first and third quartiles (box height). @ # $ % & † ‡ ⊗ ∅ Δ ∇ ∀ ∃ Ω indicate a significant pairwise difference (see Supporting information for additional statistical representations, online only).

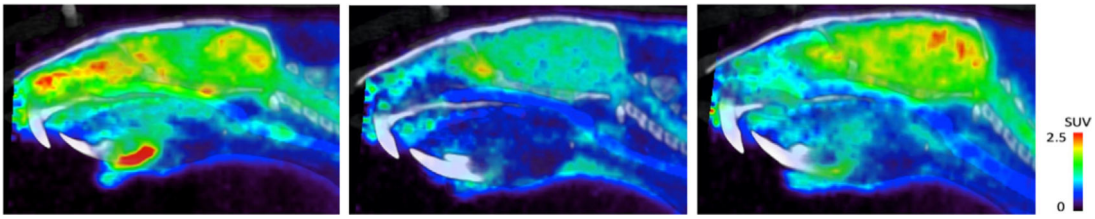

Figure 9.

PET-CT sagittal views of summed radioactivity (0–30-min) after [^{18}F]-VXS tracer injection of naive (A); POX-treated at 20 min after POX (B); and POX-treated with MINA intervention at 30 min (C); where the heat maps are as standardized uptake values (SUV) correlated to the NIH color bar defined SUV value range.

Ann N Y Acad Sci. Author manuscript; available in PMC 2020 November 22.

Table 1.

Radioactivity blood analyses in naive and POX-treated rats at 20 and 60 min postexposure ($n \geq 3$) after [^{18}F]-VXS tracer injection

Component	Time (min)					
	POX	0.5	1	5	10	30
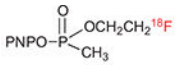 [^{18}F]-VXS (parent)	None	0.3 ± 0.1%	0.2 ± 0.1%	0.2 ± 0.1%	0.1 ± 0.1%	0.2 ± 0.1%
	20 min	0.3 ± 0.1%	0.2 ± 0.1%	0.2 ± 0.1%	0.2 ± 0.1%	0.2 ± 0.1%
	60 min	0.4 ± 0.3%	0.4 ± 0.6%	0.1 ± 0.1%	0.1 ± 0.1%	0.1 ± 0.1%
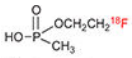 [^{18}F]-VXS metabolite*	None#	11.8 ± 1.8%	10.2 ± 2.6%	6.3 ± 1.0%	5.7 ± 0.6%	4.3 ± 0.6%
	20 min#	31.3 ± 3.0%	27.4 ± 1.4%	18.6 ± 3.3%	16.2 ± 1.1%	13.5 ± 1.4%
	60 min#	18.0 ± 0.5%	17.1 ± 1.6%	11.2 ± 0.7%	11.4 ± 1.5%	10.1 ± 1.2%
Protein fraction	None#	71.8 ± 3.5%	73.6 ± 5.4%	78.5 ± 6.7%	81.0 ± 4.5%	82.2 ± 6.0%
	20 min	48.9 ± 0.1%	50.3 ± 8.9%	54.0 ± 4.7%	58.9 ± 3.4%	59.6 ± 5.7%
	60 min	55.3 ± 15.1%	59.1 ± 3.5%	60.9 ± 8.4%	64.6 ± 7.5%	65.8 ± 5.2%
Red blood cell	None	16.1 ± 4.7%	16.1 ± 6.9%	15.0 ± 6.9%	13.2 ± 4.7%	13.3 ± 5.9%
	20 min	19.5 ± 2.8%	22.1 ± 8.3%	27.1 ± 7.5%	24.7 ± 3.4%	26.7 ± 6.6%
	60 min	26.3 ± 15.0%	23.3 ± 1.5%	27.8 ± 8.7%	23.9 ± 6.9%	24.0 ± 5.7%

*Only one metabolite observed.

#Significant change over time ($P < 0.05$).

Table 2.

Radioactivity blood analyses at 60 min in rats exposed to POX and given an oxime reactivator 30 min post-POX exposure, ($n \geq 3$) after injection of [^{18}F]-VXS tracer

Component	Time (min)					
	Oxime	0.5	1	5	10	30
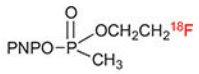 [^{18}F]-VXS parent	2-PAM	0.16 ± 0.25%	0.19 ± 0.20%	0.14 ± 0.22%	0.39 ± 0.54%	0.22 ± 0.16%
	HI-6	0.38 ± 0.35%	0.10 ± 0.05%	0.27 ± 0.14%	0.06 ± 0.03%	0.21 ± 0.13%
	MMB4	0.36 ± 0.42%	0.04 ± 0.01%	0.32 ± 0.39%	0.027 ± 0.01%	0.14 ± 0.12%
	MINA	0.29 ± 0.20%	0.14 ± 0.08%	0.14 ± 0.07%	0.11 ± 0.06%	0.16 ± 0.09%
	RS-194B	0.31 ± 0.11%	0.07 ± 0.05%	0.22 ± 0.05%	0.14 ± 0.07%	0.18 ± 0.08%
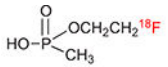 [^{18}F]-VXS metabolite*	2-PAM$^{\#}$	17.5 ± 1.7%	16.7 ± 2.4%	12.3 ± 2.4%	8.6 ± 3.5%	9.3 ± 2.2%
	HI-6$^{\#}$	21.2 ± 3.6%$^{\$}$	17.4 ± 2.1%	12.0 ± 1.1%	11.1 ± 0.5%	10.0 ± 1.7%
	MMB$^{\#}$4	25.7 ± 1.5%$^{\$}$	20.5 ± 2.8%	15.1 ± 3.2%	12.4 ± 2.4%	14.4 ± 4.0%
	MINA$^{\#}$	21.2 ± 3.6%	17.4 ± 2.1%	12.0 ± 1.1%	11.1 ± 0.5%	10.0 ± 1.7%
	RS-194B$^{\#}$	24.4 ± 3.8%$^{\$}$	17.9 ± 4.8%	11.6 ± 2.3%	10.3 ± 1.6%	10.1 ± 3.3%
Protein fraction	2-PAM	63.3 ± 4.1%	69.9 ± 2.7%	70.9 ± 4.0%	64.6 ± 14.2%	66.1 ± 6.5%
	HI-6$^{\#}$	55.9 ± 6.1%	63.7 ± 2.9%	67.0 ± 7.7%	72.3 ± 3.3%	74.9 ± 4.0%
	MMB4	56.9 ± 3.9%	62.2 ± 1.6%	67.0 ± 4.2%	59.3 ± 6.2%	62.3 ± 7.9%
	MINA	64.0 ± 2.5%	67.1 ± 3.6%	70.8 ± 3.7%	68.2 ± 7.7%	68.6 ± 6.1%
	RS-194B	60.6 ± 5.8%	61.6 ± 4.9%	66.9 ± 4.6%	71.2 ± 4.5%	66.5 ± 6.7%
Red blood cell	2-PAM	19.0 ± 3.1%	13.2 ± 2.1%	16.6 ± 3.3%	26.5 ± 14.0%	24.3 ± 7.3%
	HI-6	14.6 ± 4.3%	15.4 ± 2.2%	17.1 ± 3.2%	20.7 ± 7.7%	21.2 ± 4.4%
	MMB4	17.0 ± 2.3%	17.3 ± 3.2%	17.6 ± 2.7%	28.2 ± 5.8%	23.1 ± 3.8%
	MINA	14.6 ± 4.3%	15.4 ± 2.2%	17.1 ± 3.2%	20.7 ± 7.7%	21.2 ± 4.4%
	RS-194B	14.6 ± 2.1%	20.4 ± 9.0%	21.3 ± 6.0%	18.3 ± 2.9%	23.2 ± 3.5%

*Only one metabolite observed.

#Significant change over time ($P < 0.05$).

$Significantly different from the relevant 2-PAM values ($P < 0.05$).

Table 3.

PET radioactivity biodistribution values given as interval AUCs in naive rats framed from 0 to 5, 0 to 10, 0 to 15, and 0 to 30 min after [^{18}F]-VXS injection

	Time (min)			
Tissue	**0–5**	**0–10**	**0–15**	**0–30**
Brain (whole)	6.5 ± 0.6	13.2 ± 1.3	19.9 ± 2.0	39.6 ± 4.2
Brainstem	6.3 ± 0.6	12.5 ± 1.2	18.6 ± 1.8	36.4 ± 3.6
Cerebellum	7.6 ± 0.5	15.4 ± 1.2	23.1 ± 1.8	45.8 ± 3.9
Caudate putamen	5.5 ± 0.6	11.2 ± 1.4	16.9 ± 2.2	33.9 ± 4.1
Frontal cortex	6.1 ± 0.5	12.3 ± 1.1	18.5 ± 1.9	36.7 ± 3.9
Thalamus	5.8 ± 0.8	11.8 ± 1.7	17.7 ± 2.6	35.1 ± 5.3
Midbrain	7.5 ± 1.1	15.3 ± 1.9	23.0 ± 2.8	45.6 ± 5.5
Liver	10.3 ± 1.1	20.5 ± 2.4	30.3 ± 3.7	57.9 ± 7.0
Heart	30.2 ± 1.4	58.7 ± 2.8	86.0 ± 4.2	163.4 ± 8.3
Lung	26.1 ± 0.8	51.7 ± 1.6	76.6 ± 2.5	148.4 ± 5.2

NOTE: Data ($n \geq 3$) presented as the mean ± SD.